Journal of Materials Processing Tech. 295 (2021) 117170

Contents lists available at ScienceDirect

Journal of Materials Processing Tech.

journal homepage: www.elsevier.com/locate/jmatprotec

In-situ microstructural control of A6082 alloy to modify second phase particles by melt conditioned direct chill (MC-DC) casting process – A novel approach

K.M. Sree Manu[a,*], Nilam S. Barekar[a,b], Jaime Lazaro-Nebreda[a], Jayesh B. Patel[a,*], Zhongyun Fan[a]

[a] Brunel Centre for Advanced Solidification Technology (BCAST), Brunel University London, Uxbridge, UB8 3PH, United Kingdom
[b] Constellium University Technology Centre, Brunel University London, Uxbridge, UB8 3PH, United Kingdom

ARTICLE INFO

Associate Editor: Alan A. Luo

Keywords:
Aluminium alloys
Direct chill casting
High-shear melt conditioning
As-cast grain structure
Second phase particles
Homogenisation

ABSTRACT

Controlling the formation of noncompact second phase particles during direct chill (DC) casting of aluminium alloys with grain refiner addition remains challenging, as it results in energy intensive homogenisation and deformation problems. In this work, we employed a novel strategy in the DC casting of A6082 alloy to produce billets with a fine-scale dispersion of second phase particles. The strategy involves maintaining 2–7 °C above alloy liquidus as a thermal condition in the sump by in-situ melt conditioning (MC) using a rotor-stator high-shear device operated at a critical rotation speed. As a result, in-situ control of solidification behaviour is achieved to precisely tailor the as-cast microstructure. The billet grain refinement is attained by MC-DC casting without the deliberate addition of chemical grain refiners. The microstructure of the MC-DC cast billet at the critical rotation speed showed a fine-scale dendritic structure with refined secondary dendrite arm spacing (SDAS). The solidification front proceeded with a shallow sump and a corresponding shorter solidification time, higher cooling rate, higher temperature gradient, and smooth solidification rate profile. The ideal fine-scale dendrites with low SDAS divided the remaining eutectic liquid into fine-scale and isolated liquid pockets, resulting in fine-scale, compact morphology, and uniform distribution of second phase particles in the as-cast microstructure. The MC-DC casting process showed the ability to increase the cast house production rate by increasing the casting speed without bleeding the billet. The present approach could be beneficial for eliminating or reducing the homogenisation practice and may also introduce significant flexibility in using recycled Al alloys in the industry.

1. Introduction

Direct chill (DC) casting has been a prominent technique employed in industries to produce billets of a wide range of aluminium alloys. The vast majority of wrought aluminium alloy products begin their life cycle with DC casting to produce large billets, followed by downstream thermomechanical processing, as reported by Grandfield et al. (2013). The quality of the DC cast billets is closely dependent on its solidification microstructure in terms of (1) grain size and secondary dendrite arm spacing (SDAS), and (2) the nature of second phase particles, i.e., size, morphology, and distribution. The non-compact second-phase particles formed via eutectic or peritectic reaction during DC casting cause challenges in subsequent thermomechanical processing by raising the flow stress and ultimately lowering the quality of the products (Pradip, 2000). Therefore, in industrial practice DC cast billets are usually homogenised before thermomechanical processing to dissolve the second phase particles in the Al matrix. In addition, controlled post-homogenisation cooling is adopted to form precipitates that are easily dissolved during the subsequent thermomechanical processing. This prevents the complete solutionizing of billets, where individual solute elements can increase the flow stress, as indicated by Birol (2004). Nevertheless, among second phase particles, Fe-bearing intermetallic compounds (IMCs) in the as-cast structure cannot be dissolved during the homogenisation process (Kumar et al., 2016). This creates limitations for using recycled aluminium alloys where the Fe content in the alloy composition is beyond the target levels for downstream processing.

* Corresponding authors.
E-mail addresses: manu.kaimanikal@gmail.com (S.M. K.M.), jayesh.patel@brunel.ac.uk (J.B. Patel).

https://doi.org/10.1016/j.jmatprotec.2021.117170
Received 30 September 2020; Received in revised form 25 February 2021; Accepted 5 April 2021
Available online 8 April 2021

These problems cause practical consequences like increasing the homogenisation temperature, prolonged homogenisation time, poor surface finish, and degradation of mechanical properties of the final products.

The formation of second phase particles in the as-cast microstructure can be manipulated by controlling the solidification grain structure. McCartney (1989) reported that a more homogeneous distribution of second phase particles could be achieved by promoting a columnar to fully equiaxed transition of grain structure using Al-Ti-B(C) grain refiners (GR), i.e., chemical inoculation, where rosette type grain morphology is observed (Kumar and O'reilly, 2016). Quested and Greer (2004) indicated that during chemical inoculation, only a small fraction of the added inoculant particles (<1%) are effective for grain initiation. Consequently, the remaining inoculants accumulate in the inter-dendritic regions and cause an adverse effect on the surface finish and mechanical performance of downstream-processed components and problems for closed-loop recycling. Furthermore, elements like Zr (Wang et al., 2019) and high levels of Si (Qiu et al., 2007) in the aluminium alloys have a poisoning effect on grain refiners, making them ineffective. Alternatively, research has been conducted to impose ultrasonic (Eskin, 1994) and electromagnetic (Zuo et al., 2012 and Vanja et al., 2018) fields in the sump of the DC caster to control the grain structure, thereby reducing second phase particle dimensions, where globular type grain morphologies are observed. However, the grain structures formed in the advanced solidification processing routes in DC casting are not reliable enough to control the features of the second phase particles. Therefore, fine, compact, and uniform distribution of second phase particles need to be attained in the as-cast microstructure to shorten the homogenisation time or remove homogenisation altogether.

Fan et al. (2012) developed a novel high-shear melt conditioning (HSMC) technology at Brunel Centre for Advanced Solidification Technology (BCAST) to produce high quality DC cast billets/slab (Patel et al., 2017) without the addition of chemical grain refiners. In the melt conditioned direct chill (MC-DC) casting process, a rotor-stator high--shear device is submerged in the sump of a conventional DC caster, where the rotation of the high-shear device creates in-situ melt conditioning or shearing during casting for in-situ solidification control (Patel et al., 2014). The MC-DC technology has proven its capability in the industrial DC casting process (Li et al., 2017; Al-Helal et al., 2019, 2020, and Nilam et al., 2021) and its potential for application in many industries as a substitute for the standard grain refiners. In this study, a novel approach is implemented in the DC casting of A6082 alloy where a thermal condition of a few degrees above the alloy liquidus was maintained in the sump using the HSMC technology. Consequently, the grain structure was tailored, and the formation of second phase particles was controlled in the as-cast billet. The solidification mechanisms underlying the grain structure evolution are discussed in detail.

2. Experimental procedure

The billets were cast at BCAST lab in a vertical DC caster fitted with a hot top having an outer diameter of 134 mm, tapered inner diameter of 72–76 mm, and a height of 100 mm, followed by a graphite mould with an outer diameter of 90 mm, an inner diameter of 82 mm and a height of 55 mm. The A6082 alloy investigated in this study, with a chemical composition of Al - 1.13Si - 0.27Fe - 0.43 Mn - 0.73 Mg - 0.1Cr - 0.01Ti (all the compositions are in wt.%), was appropriately prepared by respective master alloy additions. The chemical composition was measured using optical emission spectroscopy (OES) on a Foundry Master Pro analyzer. The prepared Al alloy ingot was melted at 750 °C in an electric resistance furnace. The molten metal at 720 °C was then poured into the DC caster mould through the launder and hot-top preheated at 400 °C, followed by solidification under primary and secondary water cooling. The diameter of the DC cast billet was 81 mm. During DC casting, the billet consists of a liquid pool, slurry zone, and a mushy zone, together known as the sump, as shown in Fig. 1a. The liquid/solid transformation in the billet occurs through the slurry and mushy zones, i.e., the transition zone. For MC-DC casting, a 42 mm diameter high-shear device was preheated at 750 °C and positioned in the middle of the hot top, within the sump, at a predetermined height to introduce in-situ melt conditioning. The position of the high-shear device is schematically shown in Fig. 1a. The high-shear device comprises of a rotor and stator with small holes attached to an electric motor with a speed controller (Fan et al., 2012). The rotor consists of four blades with a diameter of 29.5 mm, and it is surrounded by a stator containing an outer diameter of 42 mm and an inner diameter of 30 mm. This provides a 0.25 mm small gap between the rotor blades and the inner side of the stator. The perimeter of the stator contains four rows of uniformly distributed 16 circular small holes having a diameter of 2.5 mm each (Fig. 1b). During the high-shear device operation, the electric motor supplies the power to the rotor through a shaft and rotates the rotor. During rotation, the rotor sucks the melt from the sump and shears the melt in the gap between the rotor and stator and ejects it at high velocity through the stator holes. The high-shear device was rotated at speeds of 1500, 2000, 2500, and 3000 rpm. The mass flow rate through the high-shear device will increase linearly with increasing rotor speed (Lebon et al., 2020). The casting speed was set at 240 or 320 mm/min, and the water flow rate at 40 L/min. The temperature of the water was at ~ 19 °C (room temperature). It should be noted that no grain refiner was added for any MC-DC casting experiments. For comparison, conventional DC casting with the addition of Optifine® (Al-3Ti-1B) grain refiner in the form of the master alloy was performed with a casting speed of 240 mm/min. The addition level of grain refiner was 1 g/kg. The thermal condition in the sump was measured using a K type thermocouple connected to a data logger to study the effect of conventional DC-GR and MC-DC castings on the evolution of the respective grain structures.

As-cast samples were used for characterization and were cut from the half radius (unless otherwise specified) of the horizontally cross-sectioned disc across the billet diameter. All the samples were sectioned from the steady-state region of the billets. The metallographic samples were prepared by mounting, polishing using grit size emery papers, final cloth polishing using colloidal silica, and then anodized using Barker's reagent for 65 s at 20 V. A Zeiss optical microscope with an AxioVision 4.3 image analysis software was used under the polarized light condition to examine the grain size and SDAS. ImageJ image analysis software was used to measure the grain size and SDAS. The grain size was measured using the line-intercept method (ASTM E112). The SDAS was assessed by measuring the distance between the centre of several adjacent dendrite arms. Scanning electron microscopy (SEM) was conducted in a Zeiss Crossbeam 340 FIB instrument to study the characteristics of second phase particles. The billet sump profile was preserved by pouring pure Zn in the hot top during conventional DC-GR and MC-DC steady state castings. Thermodynamic calculations were performed using the Pandat software package (PanAL2017 Database) under equilibrium and Scheil conditions to understand the solidification sequence of the A6082 alloy. The calculated thermodynamic parameters were also used to estimate the solidification time, as described in section 3.3.

3. Results and discussion

3.1. Thermodynamic calculations of A6082 alloy

Fig. 2 shows the changes in mass fraction of the different phases in A6082 alloy as a function of temperature based on equilibrium and Scheil calculations. The liquidus temperature of the alloy is 649.3 °C, and the solidification sequence is α-Al, Al-Fe based intermetallic compounds (IMCs), Mg_2Si and Si. Since the cooling rate during DC casting varies depending on the processing conditions and the billet size, the predicted phases may differ. Kumar and O'reilly (2016) reported the

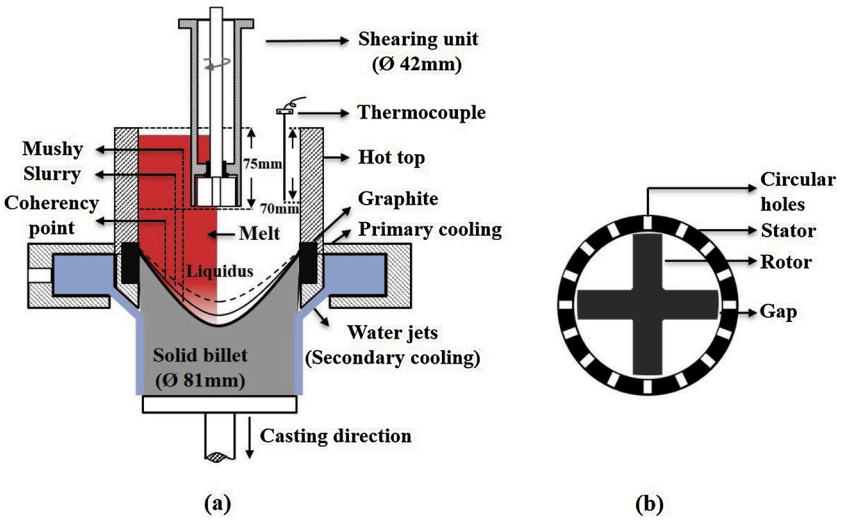

Fig. 1. Schematic representation of (a) MC-DC casting process, and (b) bottom view of the shearing unit.

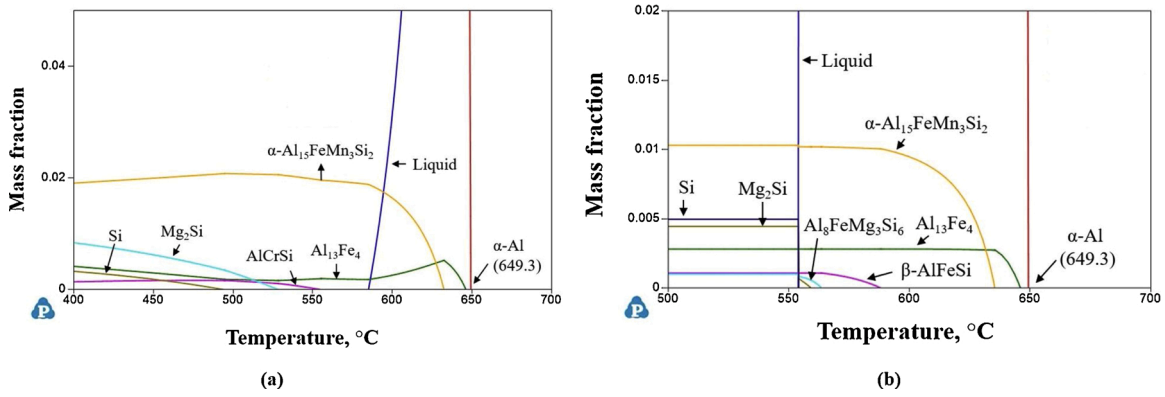

Fig. 2. Thermodynamic calculations of A6082 alloy under (a) equilibrium, and (b) Scheil conditions.

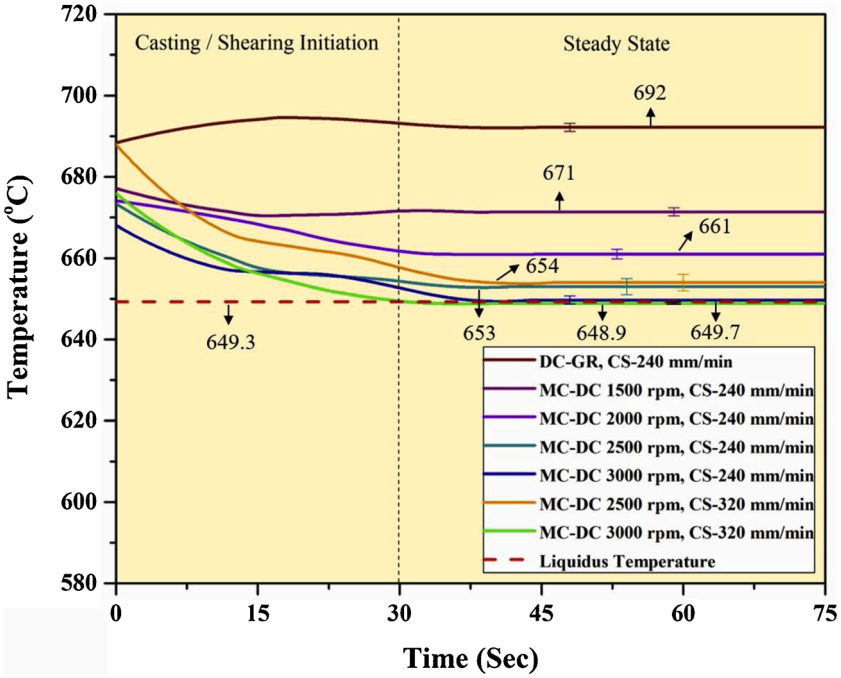

Fig. 3. Measured temperature profiles in the sump under different casting conditions.

non-existence of the $Al_{13}Fe_4$ phase in the experimental condition compared with modeling due to its transformation into α-$Al_{15}FeMn_3Si_2$ and β-AlFeSi. They further added that the phase predictions under Scheil condition are more consistent with the experiment. Of the different Al-Fe IMCs, α-$Al_{15}FeMn_3Si_2$ is the dominant phase, and by assuming the absence of the $Al_{13}Fe_4$ phase, the mass fraction of α-$Al_{15}FeMn_3Si_2$ may increase further. The age-hardenable Mg_2Si phase precipitates from the non-equilibrium segregation of solutes during the last stage of solidification. It is evident from the thermodynamic calculations that as-cast Mg_2Si will easily dissolve during solutionizing but not the α-$Al_{15}FeMn_3Si_2$ phase.

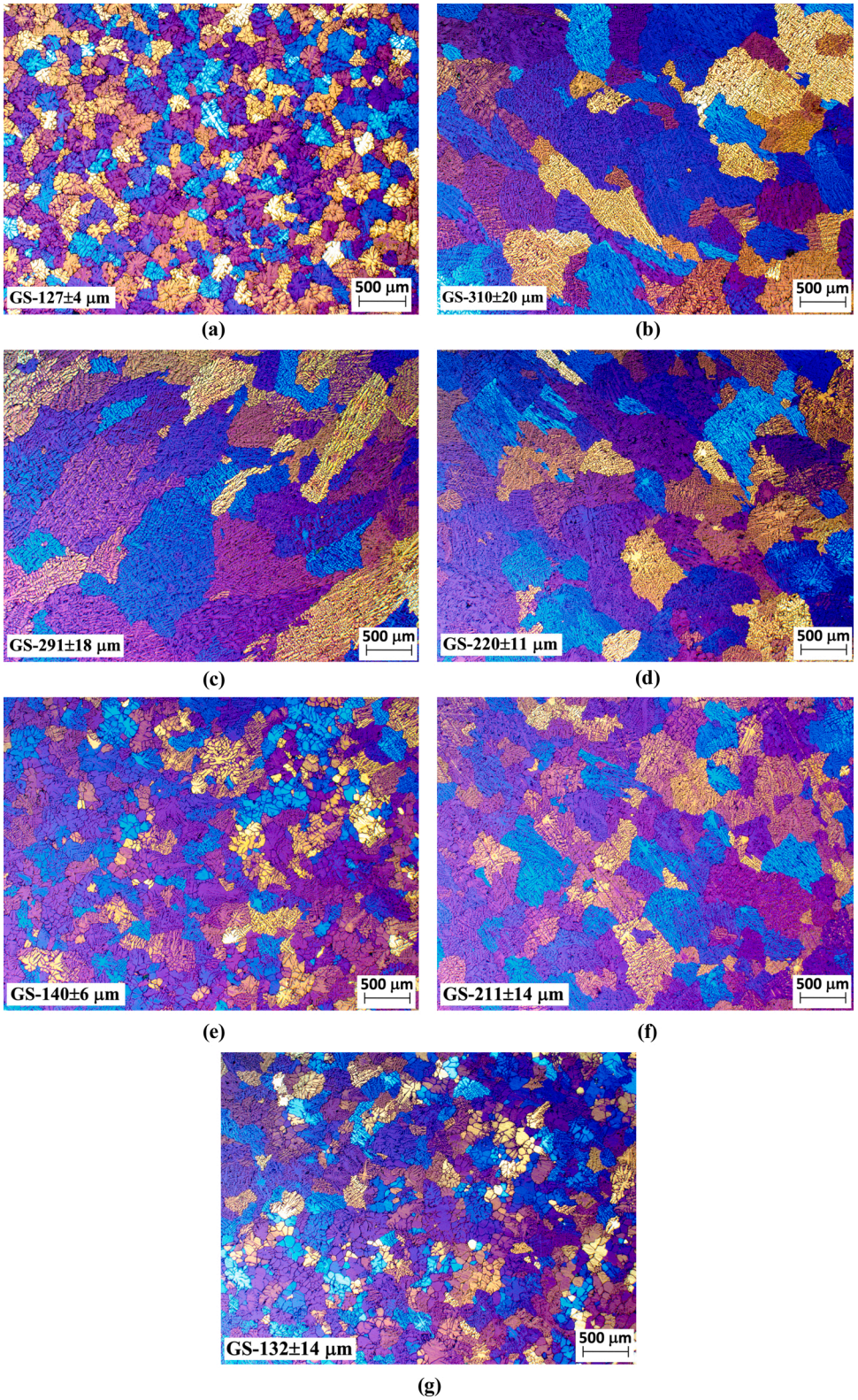

Fig. 4. As-cast microstructures of A6082 billets produced under (a) conventional DC-GR, CS-240 mm/min (b) MC-DC at a rotation speed (RS) of 1500 rpm, CS-240 mm/min (c) MC-DC at a RS of 2000 rpm, CS-240 mm/min (d) MC-DC at a critical RS of 2500 rpm, CS-240 mm/min (e) MC-DC at a high RS of 3000 rpm, CS-240 mm/min (f) MC-DC at a critical RS of 2500 rpm, CS-320 mm/min, and (g) MC-DC at a high RS of 3000 rpm, CS-320 mm/min. The corresponding grain size (GS) is indicated in each microstructure with error bars.

3.2. Effect of HSMC on temperature profile

Fig. 3 shows the temperature profiles generated in the sump during different DC casting conditions. The liquidus temperature of the A6082 alloy acts as the frontier of microstructural modification. In conventional DC-GR casting, within the sump, the temperature difference of the melt from the measured point to the liquidus line is around 43 °C, resulting from the subtraction of liquidus temperature, 649 °C, from the incoming melt temperature, 692 °C. It means a significant temperature variation is experienced in the liquid metal to reach the transition zone (slurry and mushy zone) during primary and secondary cooling. In MC-DC casting, the incoming melt temperature is systematically altered and maintained by in-situ melt conditioning within the sump using a high-shear device. During melt conditioning, the incoming melt temperature decreases rapidly. Considering the standard deviations and corresponding process parameters, the measured melt temperature difference is in the range between 21−23 °C, 11−13 °C, 2−7 °C and 2−6 °C above the liquidus, and <1 °C below the liquidus of the alloy. The profiles which are a few degrees above (2−7 °C, 2−6 °C) and below (<1 °C) the alloy liquidus maintain a uniform melt temperature (negligible variation) in the liquidus pool of the sump before reaching the transition zone. Here the focus is given to understand the effect of two specific thermal conditions in the sump, a few degrees above and just below the alloy liquidus, on the solidification structure. By controlling process parameters in MC-DC casting like the rotation speed of the high-shear device, the high-shear device position, and the casting speed (CS), the superheat temperature of the incoming melt in the sump can be precisely manipulated to a target temperature of a few degrees above or below the liquidus of A6082 alloy.

3.3. Effect of HSMC on as-cast structure

During solidification, exogenous and endogenous particles can act as potent nucleating substrates for heterogeneous nucleation. The nucleation potency depends on the degree of lattice matching at the solid/substrate interface, with smaller lattice misfit leading to higher potency. Fan (2013) developed an epitaxial nucleation model to explain the atomistic mechanism of heterogeneous nucleation on a potent substrate. The model suggests that under a critical undercooling, nucleation occurs by the epitaxial growth of a strained pseudomorphic layer on the substrate surface, followed by its transformation to a strainless solid phase. From there, solidification moves into the grain initiation or growth stage (i.e., free growth) and leads to new grain formation. Fig. 4 shows the as-cast microstructures of the billets produced by different DC casting conditions. In conventional DC-GR cast billet (Fig. 4a) at a casting speed of 240 mm/min, the formation of fully equiaxed grains are observed. The grain refiner (exogenous) in the form of master alloy contains both TiB_2 particles (lattice misfit of -4.22 pct with Al), and Al_3Ti intermetallic compound (lattice misfit of 0.09 pct with Al). The grain refinement of DC-GR cast billet can be due to (1) the increased potency of TiB_2 particles to nucleate α-Al by the formation of Al_3Ti two-dimensional compound on the TiB_2 surface during the production of grain refiner, and (2) effective growth restriction offered by the excess solute Ti in the Al melt (after the addition of grain refiner), as reported by Fan et al. (2015).

Fig. 4b–e shows the microstructures of MC-DC cast billets obtained at various rotation speeds of the high-shear device with a casting speed of 240 mm/min. At a rotation speed of 2500 rpm (Fig. 4d), fully equiaxed grains are observed. At a rotation speed of 3000 rpm (Fig. 4e), equiaxed mixed grain structures are observed. In MC-DC casting, the in-situ melt shearing provides an effective grain refinement without the necessity of grain refiner addition. Intensive melt shearing disperses and distributes the inevitable oxide films (endogenous) that exist in the Al melt into more individual particles, which significantly increases the number density of oxide particles. These particles act as potent substrates for heterogeneous nucleation of α-Al, leading to grain refinement in MC-DC cast billets. The dominant oxide formed in the investigated A6082 alloy should be $MgAl_2O_4$, according to the study by Li et al. (2012). However, the melt shearing intensity is limited at low rotation speeds, leading to a reduction in grain refinement (Fig. 4b and c). The rotation speeds of 2500 rpm and 3000 rpm show significant grain refinement compared to all other variants in MC-DC casting, so in what follows the 2500 rpm is usually referred to as the critical rotation speed and 3000 rpm as the high rotation speed (because of the resulting mixed structure). Furthermore, to understand the effect of casting speed in MC-DC cast billet, experiments were carried out at higher casting speed (320 mm/min) under critical and high rotation speeds (Fig. 4f and g). When the casting speed increases from 240 mm/min to 320 mm/min, the grain size is further refined in the billets processed under both critical and high rotation speeds. The grain refinement at higher casting speed can be linked to the subsequent increase in the solidification rate. At both critical and high rotation speeds (CS-320 mm/min), grain refinement is achieved in the MC-DC cast billets via a high enough shear rate to enhance nucleation. But the difference in rotation speed results in the evolution of different grain structures due to different thermal conditions generated in the sump. Attempts were made to employ the same casting speed for DC-GR but unfortunately resulted in a bleed out. So, the subsequent discussion will be focused on the MC-DC cast billets processed at critical and high rotation speeds under a CS of 320 mm/min with DC-GR cast billet (CS of 240 mm/min) as the reference.

The examination of duplex grain structures comprising coarse (floating grains) and fine structures are observed at the centre of the DC-GR cast billet, nevertheless, the fully fine dendritic structure is perceived at the centre of the MC-DC cast billet at critical rotation speed (Fig. 5).

It should be noted that the above experiments were carried out in an 81 mm diameter DC caster in lab-scale. For large diameter (LD) DC caster in production scale, i.e., having a large hot top and mould assembly, the corresponding shearing parameters (position of the high-shear device in the DC caster, rotation speed, etc.) and casting speed applied could be different, to attain similar thermal conditions (present study) in the sump. For instance, a case study is presented here, Fig. 6a and b shows the microstructures of A6082 (different chemical composition from the present study) conventional DC-GR and MC-DC cast billets processed in a 150 mm diameter DC caster at a casting speed of 110 mm/min. The as-cast billets processed under DC-GR contain 0.0224 Ti, and 0.0024 B, while those processed under the MC-DC have 0.0218 Ti and 0.0011 B. Optifine® (Al-3Ti-1B) grain refiner was used for DC-GR cast billets, which shows fully equiaxed grains. In MC-DC cast billet, the thermal condition in the sump is maintained 2−7 °C above the liquidus, for which the ideal rotation speed is found to be 2000 rpm to obtain fully equiaxed grains. The MC-DC cast billet from the large diameter DC caster shows enhanced grain refinement compared to the MC-DC cast billet from lab-scale DC caster processed at critical rotation speed (CS-320 mm/min), which can be attributed to the involvement of excess Ti in grain growth restriction.

The grain morphologies formed in A6082 billets under different DC casting conditions are shown in Fig. 7. In conventional DC-GR casting, a fine-scale dendritic structure but with a coarse SDAS is observed, indicating a rosette-like grain morphology. By high-shear melt conditioning, the in-situ control of solidification behaviour during casting is achieved. At the critical rotation speed (CS-320 mm/min), a fine-scale dendritic structure with refined SDAS is also observed. However, shearing at a high rotation speed (CS-320 mm/min) leads to fine-scale mixed structures with dendritic, rosette, and globular morphologies.

Fig. 8 shows the bright field optical images of conventional DC-GR and MC-DC cast billets from the large diameter DC caster, revealing similar grain morphology as in DC-GR and MC-DC cast billets (critical rotation speed, CS-320 mm/min) from lab scale DC caster.

The SDAS obtained under varying processing conditions in the DC casting of A6082 alloy is plotted in Fig. 9. It is seen that the SDAS is systematically varied by changing the rotation speed of the high-shear device. At the critical rotation speed (CS-320 mm/min), the SDAS of MC-DC cast billet is significantly finer than those obtained from other

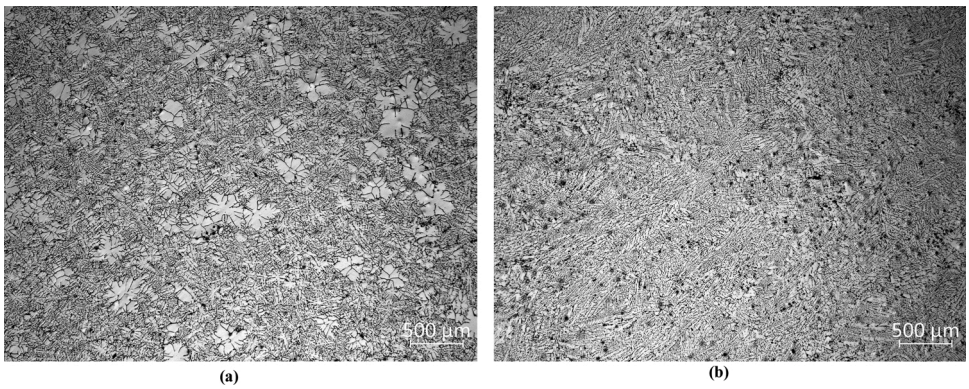

Fig. 5. As-cast microstructures at the centre of A6082 billets produced under (a) conventional DC-GR, and (b) MC-DC at critical RS.

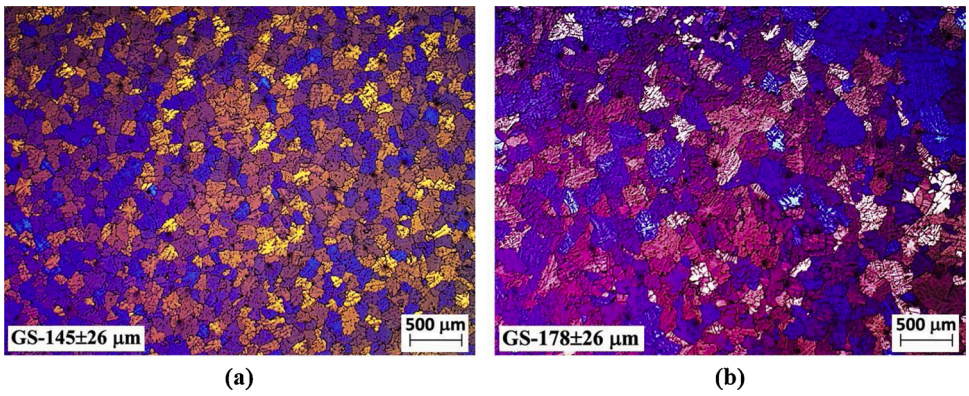

Fig. 6. As-cast microstructures of A6082 billets processed in a large diameter DC caster (Ø 150 mm) under (a) conventional DC-GR, CS-110 mm/min, and (b) MC-DC at a RS of 2000 rpm, CS-110 mm/min.

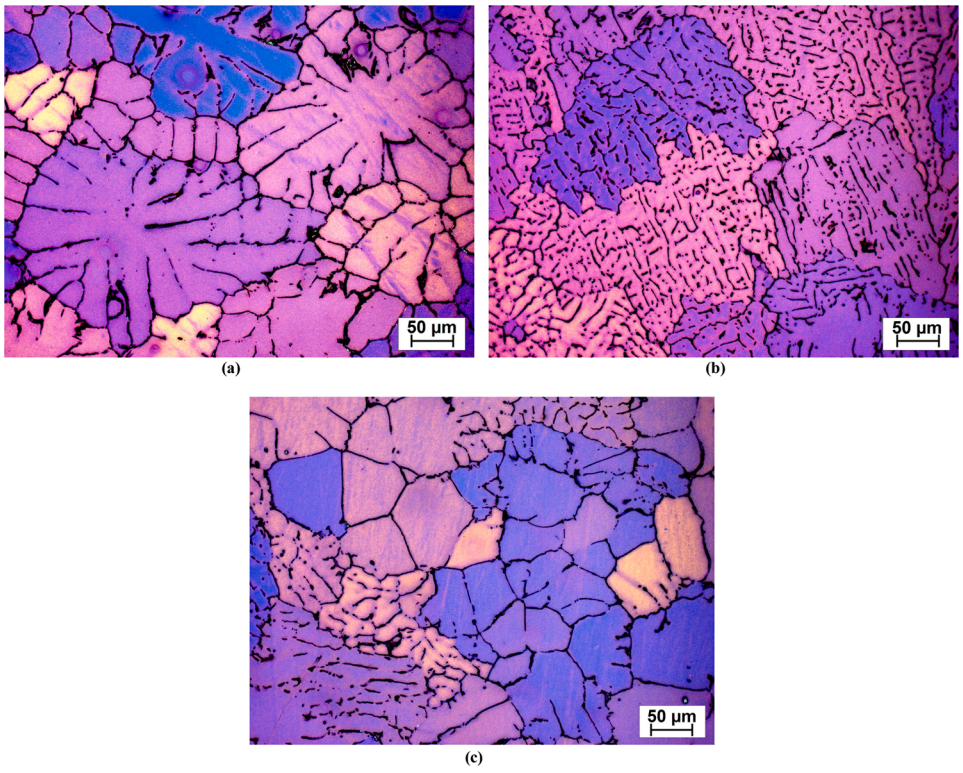

Fig. 7. High magnification microstructures revealing the development of grain morphology under varying processing conditions (a) fine-scale dendritic structure with coarse SDAS having a rosette like grain morphology in conventional DC-GR (CS-240 mm/min) (b) fine-scale dendritic structure with refined SDAS in MC-DC cast billet at critical RS (CS-320 mm/min), and (c) fine-scale mixed structures having dendritic, rosette, and globular morphologies in MC-DC cast billet at high RS (CS-320 mm/min).

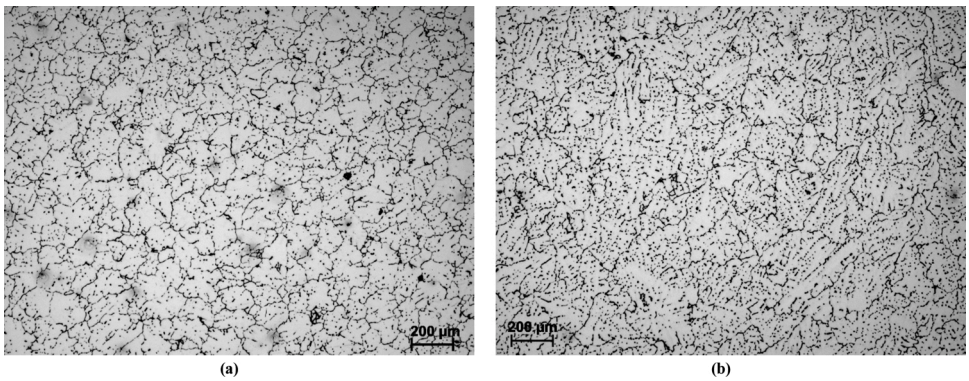

Fig. 8. Bright-field optical images showing the grain morphologies developed in (a) conventional DC-GR, and (b) MC-DC cast billets processed in large diameter DC caster (Ø 150 mm).

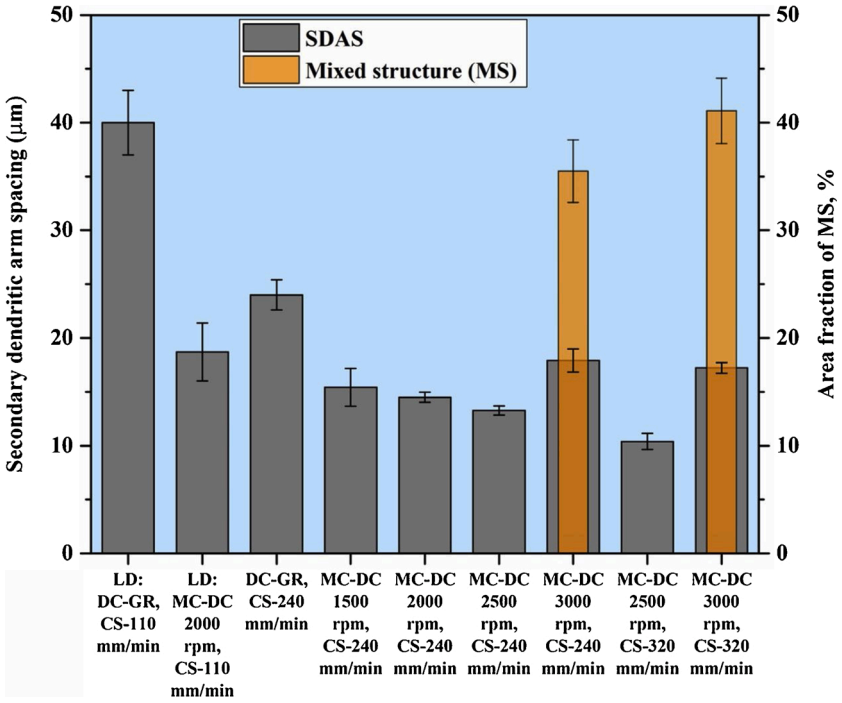

Fig. 9. Quantification of SDAS obtained under different processing conditions.

variants. When compared to conventional DC-GR cast billet, a substantial refinement is achieved by reducing the SDAS from 24 ± 1.4 µm to 10.4 ± 0.74 µm. At high rotation speed (CS-320 mm/min), the SDAS of the MC-DC cast billet is increased due to the change in grain morphology from fine-scale dendritic grains to mixed grains. The area fraction of mixed structures (rosette and globular), in which it is difficult to measure the SDAS, are also plotted. Similarly, in the case of conventional DC-GR and MC-DC cast billets from the large diameter DC caster, the SDAS of the MC-DC cast billet is much finer than DC-GR which is reduced from 40 ± 3 µm to 18.7 ± 2.7 µm, regardless of the comparable grain sizes in both cases. In addition, Easton et al. (2011) reported that the addition of solute Ti has a large effect only on grain size and not on SDAS.

The SDAS is closely related to the local solidification time, i.e., the time spent by a solid particle between the liquidus and solidus of the alloy during DC casting. Rappaz and Boettinger (1999) developed an expression for SDAS of multicomponent alloys through which SDAS can be related to the local solidification time, as follows,

$$\lambda_2 = 5.5\left(Mt_f\right)^{1/3} \tag{1}$$

$$M = \frac{-\Gamma}{\sum_{j=1}^{n} m_j\left(1-k_j\right)\left(c_{b,j}-c_{o,j}\right)/D_j} \ln\left[\frac{\sum_{j=1}^{n} m_j\left(1-k_j\right)c_{b,j}/D_j}{\sum_{j=1}^{n} m_j\left(1-k_j\right)c_{o,j}/D_j}\right] \tag{2}$$

Where, λ_2 is the secondary dendrite arm spacing (µm), and t_f *is* the solidification time (s). Γ and Dj are the Gibbs–Thompson coefficient (2×10^{-7} K m), and the diffusion coefficients in the liquid (Easton et al., 2010). k_j are partition coefficients of each solute element j in the alloy, m_j are the liquidus slopes, $c_{o,j}$ are nominal alloy concentrations, and $c_{b,j}$ are final liquid compositions (equal to the eutectic compositions). The compositional values are obtained from PANDAT software. The relationships between local solidification time, local cooling rate, and varying DC casting conditions are shown in Fig. 10. The local cooling rate can be estimated from (Spear and Gardner, 1963),

$$\log\frac{dT}{dt} = -\left(\frac{\log(DAS) - 1.66}{0.40}\right) \tag{3}$$

where dT/dt is the local cooling rate, Ks^{-1}. The MC-DC cast billet with

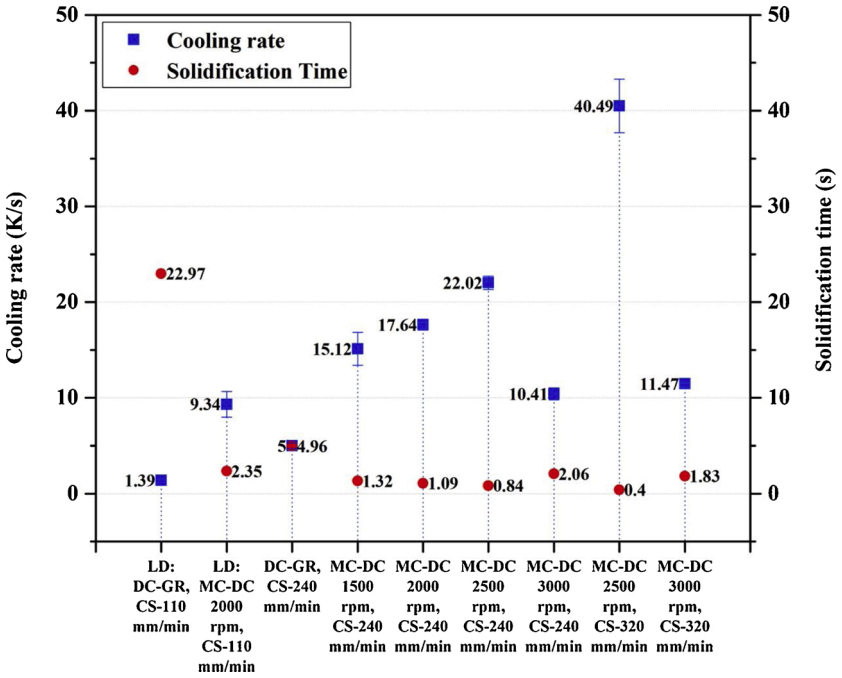

Fig. 10. The effect of different processing conditions on the cooling rate and solidification time.

low SDAS processed at the critical rotation speed (CS-320 mm/min) shows a higher cooling rate and shorter solidification time than conventional DC-GR and all other variants; the solidification time is inversely proportional to the cooling rate. From the above analysis, it is clear that the DC-GR and MC-DC (sump temperature of 2−7 °C) cast billets from both lab-scale and large diameter DC casters show the same rosette morphology and fine-scale dendrites morphology with refined SDAS. Therefore, similar fundamental factors dictate the formation of grain morphology irrespective of DC caster diameter or billet size. Subsequently, the following discussion will be limited to lab-scale DC (Ø 81 mm) billets.

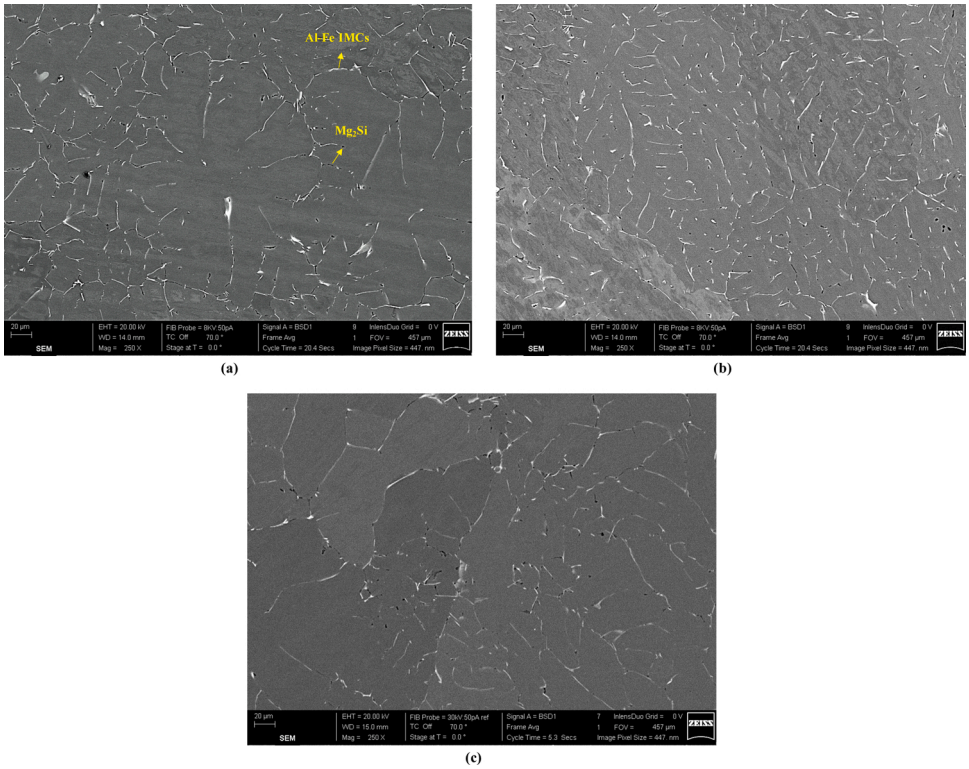

Fig. 11. SEM images showing the characteristics of second phase particles in the as-cast A6082 billets (a) interconnected network of Al-Fe IMCs and coarse Mg_2Si are formed in conventional DC-GR (CS-240 mm/min), (b) fine-scale and compact Al-Fe IMCs and Mg_2Si are formed in MC-DC cast billet at critical RS (CS-320 mm/min), and (c) interconnected network and fine-scale dispersion of Al-Fe IMCs and coarse Mg_2Si are formed in MC-DC cast billet at higher RS (CS-320 mm/min).

3.4. Effect of HSMC on second phase particles

Fig. 11 shows the SEM images of the second phase particles formed in conventional DC-GR and MC-DC cast billets. It is evident from the images that the size, morphology, and distribution of second phase particles in the as-cast microstructure depend on the grain morphology. The formation of Al-Fe IMCs (white) and the precipitation of Mg_2Si (black) can be perceived. In DC-GR cast billet (Fig. 11a) having fine-scale dendritic grains with coarse SDAS, an interconnected network of Al-Fe IMCs is observed. This is because the solute elements rejected by the growth of rosette grain morphology will be accumulated in the inter-dendritic region, leading to the formation of interconnected large eutectic pockets or open eutectic channels surrounding the α-Al dendrites at the last stage of solidification. Therefore, intermetallics nucleate and grow associated with the continuous eutectic liquid channels resulting in large Al-Fe IMCs with a non-compact morphology. In MC-DC cast billet (Fig. 11b), having a fine-scale dendritic structure with low SDAS, Al-Fe IMCs have a small size, compact morphology, and a uniform distribution. Here, the growth of ideal fine-scale dendrites with thin arms divides the remaining eutectic liquid into fine-scale and isolated liquid pockets (in-between the thin α−Al dendrite arms) at the last stage of solidification. This facilitates the homogeneous distribution of rejected solute elements, resulting in more sites for intermetallic formation. Solidification of such eutectic liquid pockets under a high cooling rate produces fine-scale and compact Al-Fe IMCs throughout the Al matrix owing to the space confinement and a limited supply of liquid. In MC-DC cast billet (Fig. 11c) with fine-scale mixed grain structures, the interconnected network and fine-scale dispersion of Al-Fe IMCs are observed, with the former being dominant due to the supremacy in the growth condition of the relevant grain morphology. The MC-DC cast billet with fine-scale dendrites as well as low SDAS shows fine-scale and uniform distribution of Mg_2Si precipitates compared to the other two variants.

Fig. 12 shows the maximum Feret diameter of Al-Fe IMCs and Mg_2Si precipitates in DC-GR and MC-DC cast billets. The measurements are obtained by SEM image analysis using ImageJ software. The Al-Fe IMCs and Mg_2Si in MC-DC cast billet (2500 rpm at CS-320 mm/min) are smaller in size, and the size distribution of Al-Fe IMCs is narrower, compared to other casting conditions.

3.5. Effect of HSMC on sump characteristics

The macrographs of the billet sump profile obtained during conventional DC-GR and MC-DC castings are shown in Fig. 13. A dotted line has been drawn in the images to highlight the sump profile (Al-Zn interphase) in each case. In the DC-GR cast billet at a casting speed of 240 mm/min (Fig. 13a), the sump profile looks smooth (no appreciable defects) and exhibits the typical kind of parabolic shape. When the casting speed is increased to 320 mm/min in the DC-GR cast billet casting (Fig. 13b), the sump gets deeper and severe cracks are observed within the sump, towards the edge, and along the centre of the billet. It is well known in DC casting that as casting speed increases, the solid network at the outer periphery of the billet (i.e., billet shell) becomes thinner as the removal of heat is reduced. This causes tendency towards horizontal cracking and bleed-out. This kind of bleed-out happened during the casting of the billet shown in Fig. 13b, as the shell formation rate failed to cope with the billet casting speed. In the case of MC-DC cast billet at the critical rotation speed and casting speed of 320 mm/min (Fig. 13c), the sump looks again smooth, similar to DC-GR cast billet at low speed (Fig. 13a), and becomes shallower than for the DC-GR cast billet with the same casting speed (Fig. 13b). Moreover, no cracking or bleed-out happened during MC-DC casting at the evaluated rotation speed. This indicates the MC-DC casting process capability to enhance the cast house production rate by increasing the casting speeds without bleeding the billet.

An increase in the casting speed from 240 to 320 mm/min during the DC-GR casting process changes the sump depth from 83 to 112 mm. In the MC-DC casting process, however, the sump shape at a casting speed of 320 mm/min becomes shallower, with the sump depth only increased to 95 mm, thus smaller than the corresponding for the DC-GR cast billet. Eskin (2008) showed that the depth of the billet sump (H) is related to the casting speed (V_{cast}) through expression (Eq4), where R is the billet radius and A is a constant that depends only on the physical properties of the alloy and the cooling conditions.

$$H = AR^2V_{cast} \tag{4}$$

From the calculated depths of the sumps in Fig. 13 we obtained a value of A = 0.348 for the case of DC-GR cast billets and a lower value A = 0.297 for the case of MC-DC cast billet. The solidification rate (V_s) i.e., the solidification front velocity in the billet depends on the casting speed (V_{cast}) according to the following relation, from Eskin (2008).

$$V_s = V_{cast}\cos\alpha_n \tag{5}$$

where α_n is the angle between the axis of billet and normal to the solidification front. This means the solidification rate is a function of the shape of the sump profile and is maximum at the centre of the billet and high near the periphery of the billet, where the sump shape is more horizontal. The sump profiles (depth as a function of distance to centre) are obtained by using ImageJ image analysis software to extract the coordinates of the points along the dotted lines shown in Fig. 13. Fig. 14a shows the obtained sump profiles for the three billets, together with a schematic of the relation between V_s and V_{cast} described by Eq. 5. In order to obtain more accurate values of α_n along the "dotted" sump

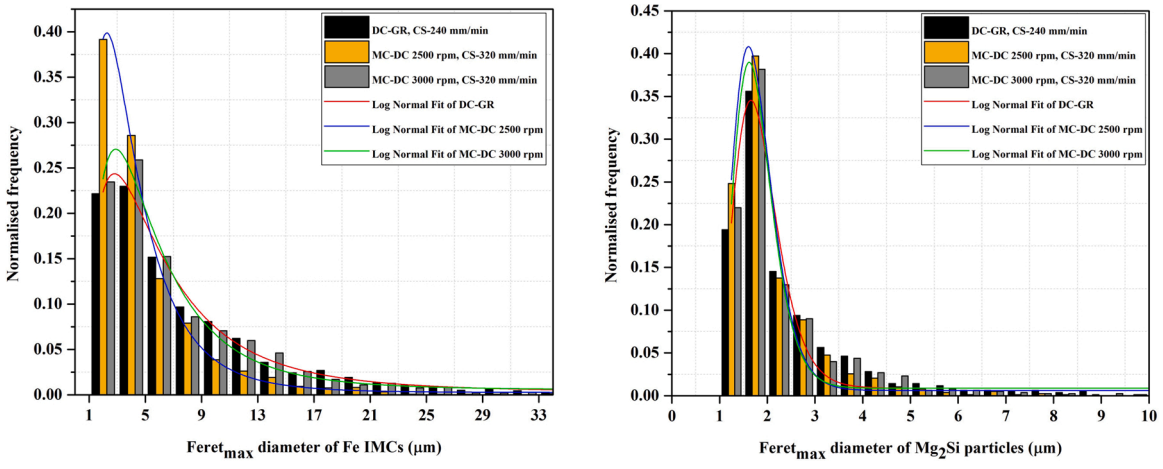

Fig. 12. Quantitative analysis of second phase particles in the as-cast billets.

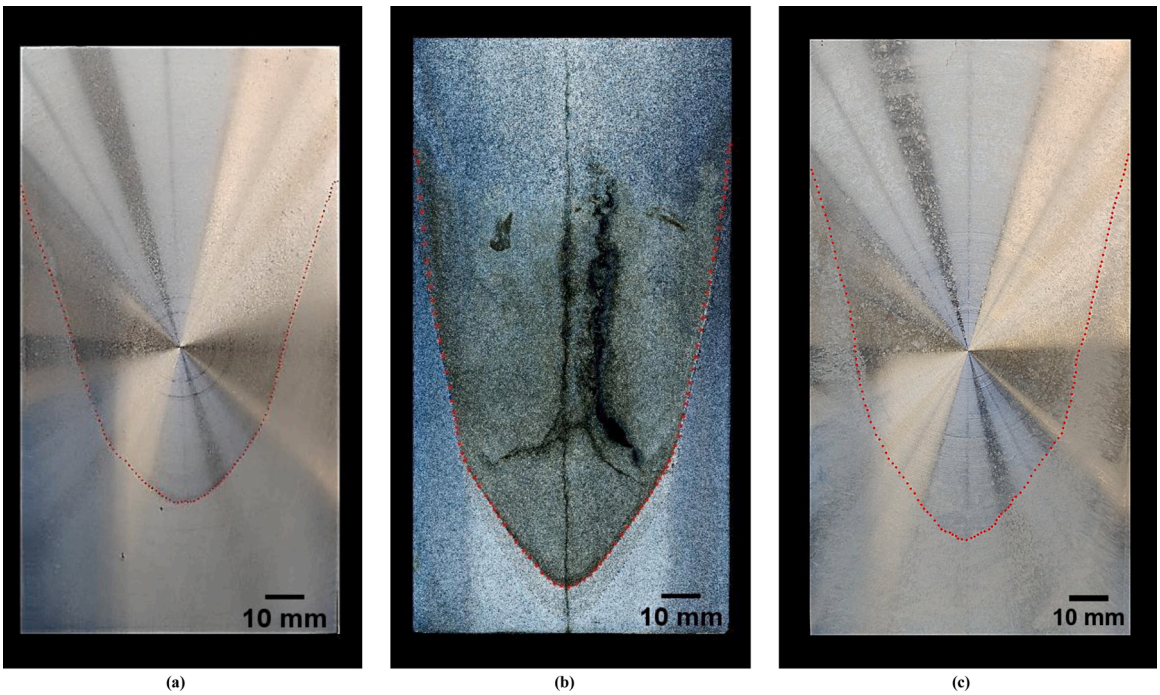

Fig. 13. Macrographs of the sump profile under (a) DC-GR, CS-240 mm/min (b) DC-GR, CS-320 mm/min, and (c) MC-DC at critical RS, CS-320 mm/min.

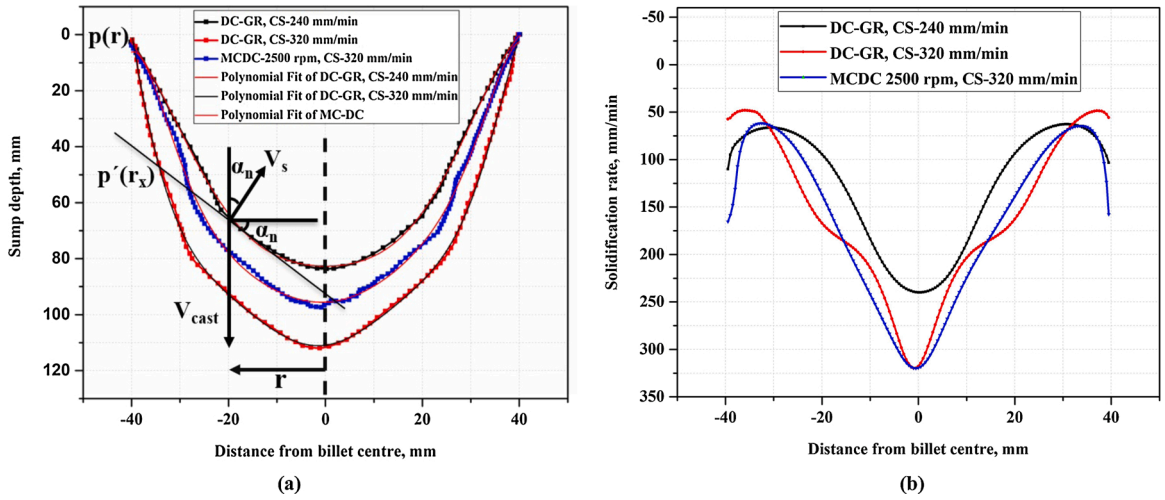

Fig. 14. (a) Measured sump profiles (dotted), with polynomial fittings (lines), and (b) corresponding solidification rate versus distance from billet centre for the selected DC-GR and MC-DC cast billets, calculated through the expression $V_s = V_{cast}\cos\alpha_n$.

profile, the set of points are smoothed and fitted by polynomial (p) regression. Each sump profile is modelled by a polynomial of degree 8, included in Fig. 14a as solid lines, with coefficients of determination (R-square) above 0.995 in all cases. These fittings, p(r), are used to obtain the value of α_n, by taking into account that at each point at distance r_x from the centre of the billet, it is satisfied that $\tan(\alpha_n) = p'(r_x)$. The solidification rate of DC-GR and MC-DC cast billets is shown in Fig. 14b. It increases with an increase in the casting speed, as expected from Eq. 5, and exhibits the typical maximum at centre and near the billet surface. The solidification rate profiles from the surface to the centre of the billets, along the horizontal direction, exhibit some differences when the three billets are compared. Firstly, the solidification rate at the periphery of the DC-GR (CS-240 and 320 mm/min) and MC-DC (critical rotation speed at CS-320 mm/min) cast billets under primary cooling are 110, 56, and 165 mm/min, respectively. This, on one hand, clarifies the reason for the bleed out during DC-GR casting at a higher casting speed of 320 mm/min and, on the other hand, highlights the higher removal of heat in the case of MC-DC casting and its potential to increase production rate. Secondly, as we move towards the centre of the billet, the solidification rate decreases to a similar value in the subsurface region under all the casting conditions due to the low heat extraction caused by the formation of an air gap (a zone between the primary and secondary cooling). Thirdly, a continuous increase in the solidification rate towards the inner layer occurs due to secondary cooling, where water jets directly hit the billet surface. In this region, the increase of casting speed in DC-GR cast billets causes the appearance of shoulders in the solidification rate profile, probably due to the inhomogeneities in melt temperature and heat extraction along the sump. In the case of MC-DC casting, a smoother increase in the solidification rate is observed from the airgap-affected region towards the centre of the billet, because of the homogeneity in melt temperature and smoother solidification front.

3.6. Solidification mechanism in DC-GR casting

In conventional DC casting, solidification of the billet takes place under primary and secondary cooling. The primary cooling (graphite) helps to form a solid outer shell of the billet followed by the withdrawal of billet from the DC caster mold, and the secondary cooling (water jets) facilitates solidifying the inner core of the emerging billet to form a bulk ingot. Sengupta et al. (2005) reported that more than 80 % of the total heat is released by secondary cooling. Generally, in DC casting, the cooling rate decreases from the edge to the centre of the billet cross-section. The grain structure evolution in DC casting is influenced by the slurry and mushy zone. The cooling rate in the slurry zone depends on the incoming melt temperature, and the heat transfer mechanism is by convection. In the mushy zone, the cooling rate is higher through the conduction mechanism.

As the secondary cooling progresses in conventional DC-GR casting (CS-240 mm/min), Fig. 15, the melt temperature reaches below the liquidus temperature; subsequently, nucleation occurs on the inoculant particles creating a local solid-liquid slurry region in the sump. The growth of a new crystalline phase starts on an inoculant particle at a particular undercooling, which is inversely proportional to the particle diameter (Greer et al., 2000). The crystals grow from different directions and collide upon one another, building a continuous coherency structure from where the mushy zone begins, followed by its transformation to solid billet. In commercial wrought aluminium alloys used in DC casting the transition of the slurry zone into the mushy zone is between a solid fraction of 0.2 and 0.33 (Nadella et al., 2008). The heat transfer in the slurry zone occurs through natural thermo-solute convection, and in the mushy zone, the formation of coherency structure causes the heat transfer mainly through conduction. The natural convection creates a descending melt flow at lower velocity along the solidification front in the outer quarter of the sump, and then rises in the centre of the billet. The rise of melt in centre portion might be due to the momentum caused by the sinking of cooler liquid at the periphery of the billet, as indicated by Eskin et al. (2011). The melt flow in the slurry zone, closer to the billet surface, continuously supplies the fresh melt containing inoculant particles from the liquidus pool. Meanwhile, the melt flow transports the nucleated solid crystals resulting in grain floating and settlement. Therefore, a coupling effect between nucleation, growth, and flow is created in the sump. The nucleation rate in a localized region is mainly influenced by undercooling. But it also depends on the melt flow rate i.e., a higher flow velocity supplies the inoculant particles at a higher rate (Combeau et al., 2016).

Considering the sump characteristics, the high melt temperature variation (43 °C) to reach the transition zone causes enlargement of the sump (liquid, slurry, and mushy zones) depth and width due to the increase in the total heat extraction through the surface of the billet. The growing nuclei release latent heat and ultimately cause the rise in temperature of the slurry zone, called recalescence, further extending the slurry zone of DC-GR casting. This all results in a lower temperature gradient, lower cooling rate, and longer solidification time in the slurry zone. Hence, nucleated grains grow in the form of dendrites at a lower velocity in the above-characterized slurry zone, followed by final grain development in the mushy zone, leading to a rosette like grain morphology with a coarse SDAS. Consequently, the interconnected network of large Al-Fe IMCs and coarse Mg_2Si is formed in the as-cast DC-GR cast billet. High-temperature homogenization is then required to dissolve the second phase particles before downstream deformation processing, and some proportion of the α-Fe IMCs are known to survive the homogenisation process.

3.7. Solidification mechanism in MC-DC casting at critical rotation speed and CS-320 mm/min

In MC-DC casting, the billet grain refinement is attributed to the oxide/inclusion particles in the aluminium melt, thereby converting the harmful oxide bi-films to potent nucleants. The intensive in-situ melt shearing during DC casting generates forced convection in the sump (Fig. 16), resulting in enhance mass transport and heat transfer in the liquidus pool and slurry zone due to the macroscopic melt flow at higher velocity. It overwhelms the relative movement of the solid and liquid phases during solidification. This rapid melt flow also supplies the nucleation substrates at a high rate and transports the nucleated solid crystals faster. At critical rotation speed (CS-320 mm/min), the high shear device sucks the colder melt from the lower portion of the sump (casting direction), followed by its mixing and redistribution with an incoming melt at a temperature of 692 °C. This process enables the formation of a liquidus pool with a uniform melt temperature. It maintains a temperature difference of 2−7 °C above the liquidus of the alloy (T_{sump}= ~654 °C), in this case, $T_{sump} > T_{Liquidus}$. Under secondary cooling, since the melt temperature variation to reach the transition zone is very low, the sump (liquid, slurry, and mushy zone) gets shallow due to the decrease in the total heat extraction. This reduces the thickness of the transition zone; obviously, the slurry zone becomes well narrow, resulting in a higher temperature gradient, higher cooling rate, and shorter solidification time in the slurry zone. In other words, the

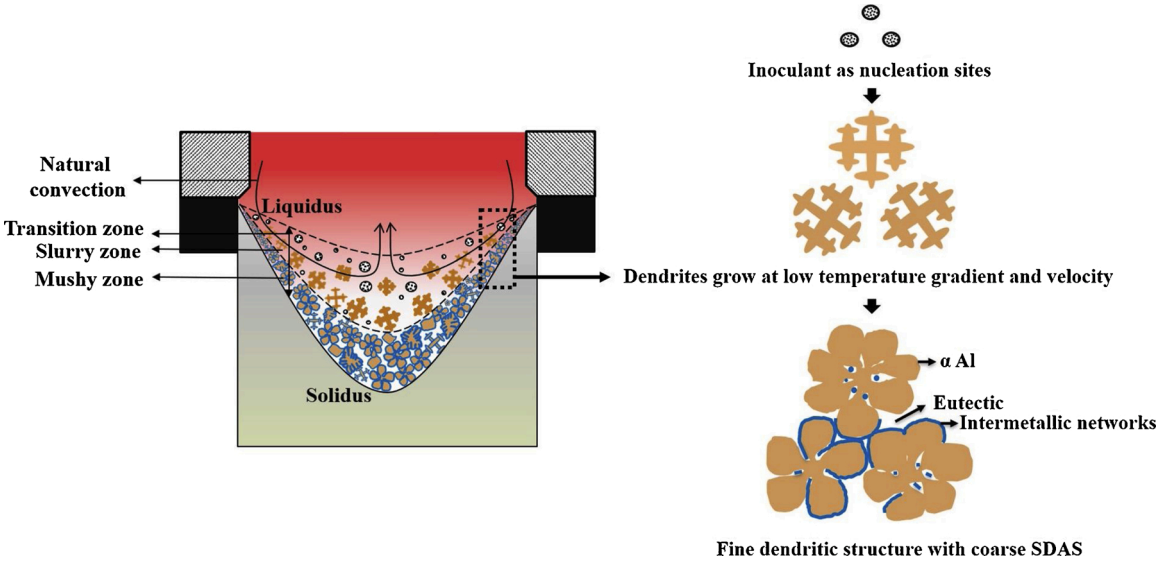

Fig. 15. Schematic of the solidification mechanism causing the grain structural evolution during DC-GR casting under natural convection.

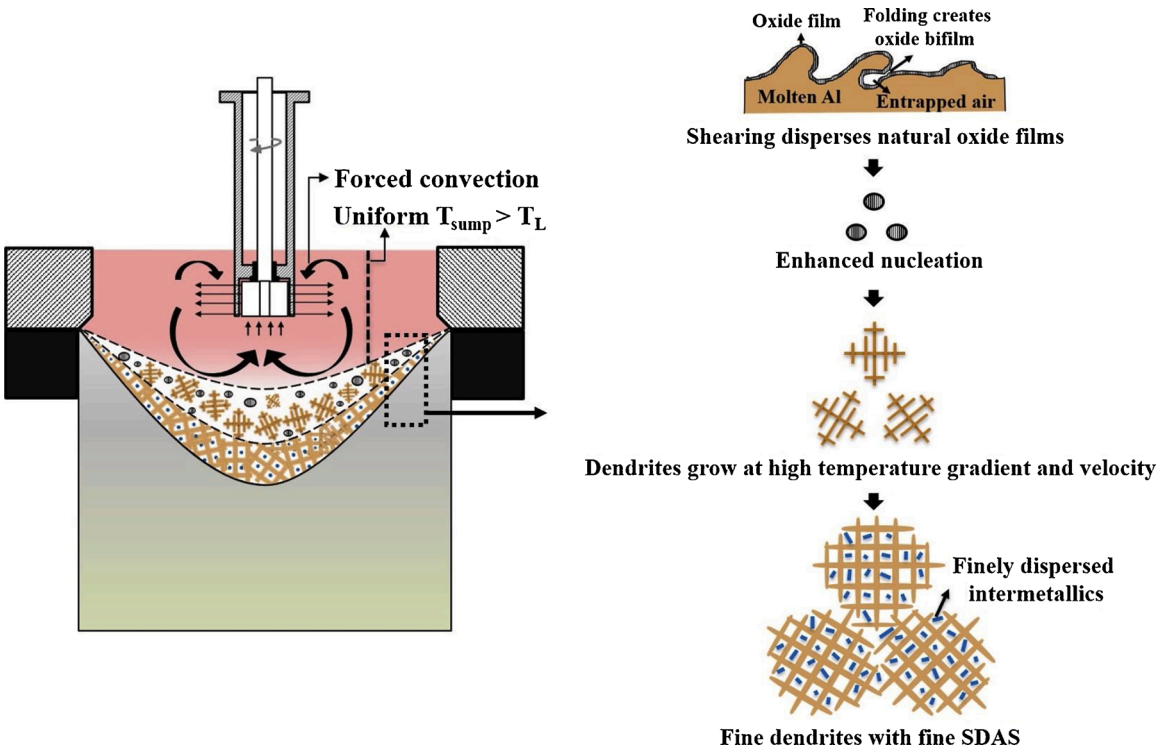

Fig. 16. Schematic of the solidification mechanism causing the grain structural evolution during MC-DC casting at critical rotation speed (CS-320 mm/min) under forced convection.

solidification front in the transition zone is characterised by a higher temperature gradient. Therefore, nucleated grains grow in the form of dendrites at a faster growth rate leading to a fine-scale dendritic structure with low SDAS. Consequently, fine-scale compact Al-Fe IMCs and Mg_2Si are formed uniformly throughout the Al matrix of as-cast MC-DC cast billet, and high-temperature homogenisation can be reduced or even eliminated.

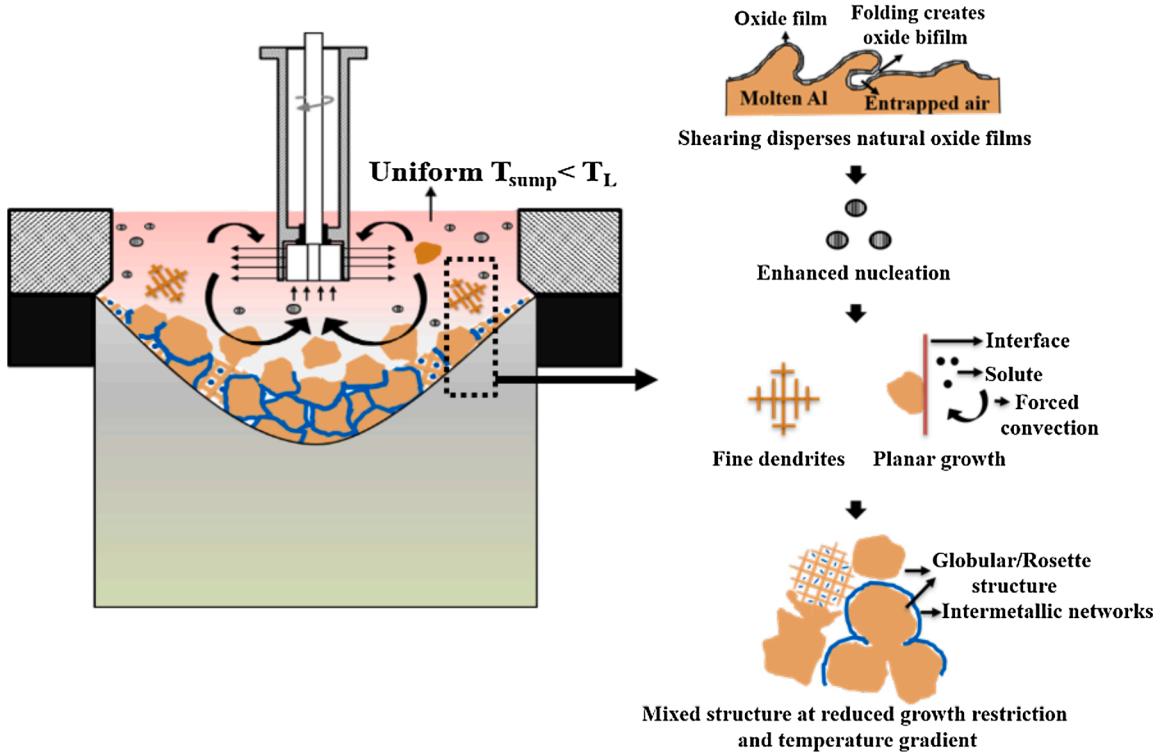

Fig. 17. Schematic of the solidification mechanism causing the grain structural evolution during MC-DC casting at high rotation speed (CS-320 mm/min) under forced convection.

3.8. Solidification mechanism in MC-DC casting at high rotation speed and CS-320 mm/min

At high rotation speed (CS-320 mm/min), Fig. 17, the upward flow of colder melt is enormous in such a way that it forms a liquidus pool with uniform melt temperature, but it maintains a temperature just below the liquidus of the alloy (T_{sump}= ~ 648.9 °C), in this case, $T_{sump} < T_{Liquidus}$. Therefore, here the liquidus pool will convert into a large slurry zone. Under this condition also, the sump becomes shallow; however, the formation of a large slurry zone with a temperature just below the liquidus creates a lower temperature gradient, lower cooling rate, and longer solidification time. Both nucleation and growth occur in the sump (large slurry zone) under forced convection, leading to a fine-scale mixed grain structure with dendritic, rosette, and globular morphologies. The possible mechanisms that can be proposed for the mixed structures are (i) dendritic morphology due to local short solidification time (ii) globular morphology caused by the planar growth front due to the removal of solute diffusion area around the growing solid by the forced convection (iii) rosette morphology due to reduced growth restriction which causes the dendrites to coarsen and leads to globular morphology. Consequently, the mixture of interconnected, fine-scale, and coarse second phase particles are formed in the as-cast MC-DC cast billet.

3.9. MC-DC casting window

Apart from rotation speed, the casting speed and high-shear device position play an important role in altering the sump temperature 2−7 °C above the alloy liquidus during MC-DC casting. Increasing the casting speed deepens the sump, which makes the colder liquid zone away from the vicinity of the sucking action of the high-shear device. This was the case with a critical rotation speed at a CS of 240 and 320 mm/min. However, when the high-shear device runs at a high rotation speed, the sump is disturbed profoundly so that the effect of the casting speed is less active, as in the case of high rotation speed at a CS of 240 and 320 mm/min. A higher position of the high-shear device, away from the transition zone, lowers both the upward flow of colder melt and the risk of having the device solidify inside the billet. Fig. 18 illustrates the optimum temperature difference in the sump characterising the casting window (dashed rectangle) as a function of high-shear device rotation speed and casting speed. We have employed the nearest-neighbor approach to interpolate the scattered initial values of temperature difference, rotation speed, and casting speed. The algorithm first computes the Delaunay triangulation in the 2-dimensional approach (casting speed vs temperature difference) for RS = 0 and then uses the associated Voronoi polygons to interpolate the RS-value for any point within the domain. The Voronoi diagrams were computed using Igor Pro version 8.04. The current approach is used for the 81 mm diameter DC cast mould but can be easily extended to variety of other DC caster mould diameters.

4. Conclusions

A novel approach is proposed in the direct chill (DC) casting of A6082 alloy using melt conditioning technology with a rotor-stator high-shear device. This new approach allows the possibility of eliminating or reducing the need for homogenisation, and increases the flexibility of using recycled Al alloys, with increased production rates in industrial cast houses. The major conclusions are:

- Grain refinement is achieved in the A6082 billet by melt conditioned direct chill casting (MC-DC) without the deliberate addition of grain refiners (GR), which can be attributed to the heterogeneous nucleation of α-Al on the dispersed natural oxide particles (endogenous) in the melt.
- The melt temperature in the sump during DC casting is manipulated by in-situ high-shear melt conditioning within the sump using a rotor-stator device operated at a selected rotation speed, thereby tailoring the as-cast grain structure of the A6082 alloy billet.

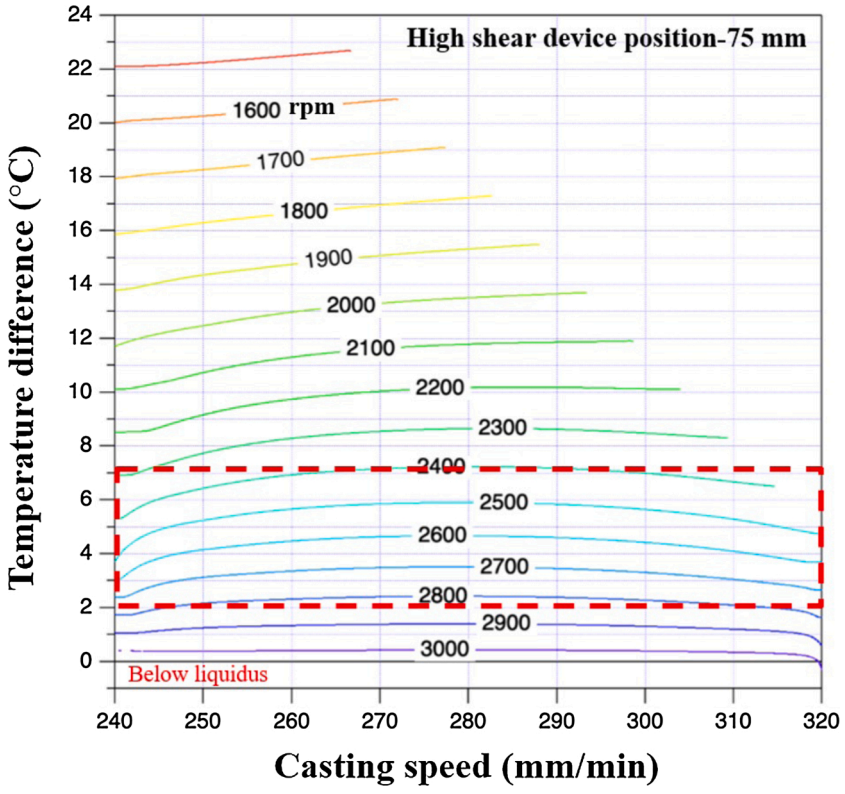

Fig. 18. The predicted optimum temperature difference in the DC casting sump indicating the casting window (dashed rectangle) as a function of high-shear device rotation speed and casting speed, obtained using Voronoi diagrams.

- During MC-DC casting at a critical rotation speed, a thermal condition of 2–7 °C above alloy liquidus is maintained in the sump which results in a fine-scale uniform equiaxed dendritic structure with refined secondary dendrite arm spacing (SDAS).
- During MC-DC casting at a high rotation speed, the thermal condition in the sump reach below the liquidus of the alloy which results in fine-scale mixed structures with dendritic, rosette, and globular morphologies. A fine-scale dendritic structure with coarse SDAS is observed in the conventional DC-GR cast billet indicating rosette morphology.
- At the critical rotation speed, the solidification proceeded with a shallow sump and a shorter solidification time, higher temperature gradient, and higher cooling rate than the other two variants.
- The growth of ideal fine-scale dendrites with low SDAS divided the remaining eutectic liquid into fine-scale isolated liquid pockets at the last stage of solidification. Solidification of such eutectic liquid pockets under a high cooling rate produced a fine-scale, compact morphology, and a uniform distribution of second phase particles in the as-cast microstructure.
- This contrasts with the case of mixed and rosette morphologies for the MC-DC at high rotation speed and for the DC-GR, where interconnected large eutectic pockets create secondary phase particles with a non-compact network like morphology.
- At the critical rotation speed, the MC-DC casting made it easier to increase the casting speed without causing bleed out, whereas a crack and bleed out are observed in the DC-GR cast billet at higher casting speed.
- A smooth solidification rate profile is observed in the MC-DC casting at the critical rotation speed. The solidification rate is a function of the shape of the sump profile and increases with the casting speed. The increase is at a maximum at the centre of the billet and is high near the periphery of the billet.
- The casting speed and high-shear device position also plays a vital role in altering the sump temperature to a few degrees above the alloy liquidus during MC-DC casting.

CRediT authorship contribution statement

K.M. Sree Manu: Conceptualization, Methodology, Software, Validation, Formal analysis, Investigation, Visualization, Writing - original draft, Writing - review & editing. **Nilam S. Barekar:** Methodology, Validation, Investigation, Writing - review & editing. **Jaime Lazaro-Nebreda:** Methodology, Formal analysis, Writing - review & editing. **Jayesh B. Patel:** Conceptualization, Methodology, Validation, Investigation, Visualization, Resources, Supervision, Writing - review & editing. **Zhongyun Fan:** Conceptualization, Supervision, Project administration, Funding acquisition, Resources, Writing - review & editing.

Declaration of Competing Interest

The authors report no declarations of interest.

Acknowledgements

The Engineering and Physical Sciences Research Council (EPSRC) of the UK and Constellium (UK) are gratefully acknowledged for providing financial support under the STEP Al prosperity partnership grant (EP/S036296/1). Prof. Brian Cantor, Dr. Chamini Mendis, Dr. Farsad Forghani, and Dr. Maaouia Souissi are thanked for their technical assistance and stimulating discussions.

References

Al-Helal, K.W., Lazaro-Nebreda, J., Patel, J.B., Scamans, G.M., Fan, Z., 2019. Melt conditioned direct chill (MC-DC) casting of AA-6111 aluminium alloy formulated from incinerator bottom ash (IBA). Recycling 4, 37.
Al-Helal, K.W., Patel, J.B., Scamans, G.M., Fan, Z., 2020. Melt conditioned direct chill (MC-DC) casting and extrusion of AA5754 aluminium alloy formulated from recycled taint tabor scrap. Materials 13, 2711.
Birol, Y., 2004. The effect of homogenization practice on the microstructure of AA6063 billets. J. Mater. Process. Technol. 148, 250–258.
Combeau, H., Založnik, M., Bedel, M., 2016. Predictive capabilities of multiphysics and multiscale models in modeling solidification of steel ingots and DC casting of aluminum. JOM. 68, 2198–2206.
Easton, M., Davidson, C., StJohn, D., 2010. Effect of alloy composition on the dendrite arm spacing of multicomponent aluminum alloys. Metall. Mater. Trans. A 41, 1528–1538.
Easton, M., Davidson, C., StJohn, D., 2011. Grain morphology of As-Cast wrought aluminium alloys. Mater. Trans. 52, 842–847.
Eskin, G.I., 1994. Influence of cavitation treatment of melts on the processes of nucleation and growth of crystals during solidification of ingots and castings from light alloys. Ultrason. Sonochem. 1, S59–S63.
Eskin, D.G., 2008. Physical Metallurgy of Direct Chill Casting of Aluminum Alloys. CRC Press/Taylor & Francis, Boca Raton, pp. 91–92.
Eskin, D.G., Jafari, A., Katgerman, L., 2011. Contribution of forced centreline convection during direct chill casting of round billets to macrosegregation and structure of binary Al–Cu aluminium alloy. Mater. Sci. Technol. 27, 890–896.
Fan, Z., 2013. An epitaxial model for heterogeneous nucleation on potent substrates. Metall. Mater. Trans. A. 44, 1409–1418.
Fan, Z., Zuo, Y.B., Jiang, B., 2012. Apparatus and Method for Liquid Metals Treatment. WO2012035357A1.
Fan, Z., Wang, Y., Zhang, Y., Qin, T., Zhou, X.R., Thompson, G.E., Pennycook, T., Hashimoto, T., 2015. Grain refining mechanism in the Al/Al–Ti–B system. Acta Mater. 84, 292–304.
Grandfield, J.F., Eskin, D.G., Bainbridge, I.F., 2013. Direct-Chill Casting of Light Alloys: Science and Technology. John Wiley & Sons, New Jersey.
Greer, A.L., Bunn, A.M., Tronche, A., Evans, P.V., Bristow, D.J., 2000. Modelling of inoculation of metallic melts: application to crystal refinement of aluminium by Al-Ti-B. Acta Mater. 48, 2823–2835.
Kumar, S., O'reilly, K.A.Q., 2016. Influence of Al grain structure on Fe bearing intermetallics during DC casting of an Al-Mg-Si alloy. Mater. Charact. 120, 311–322.
Kumar, S., Grant, P.S., O'reilly, K.A.Q., 2016. Evolution of Fe bearing intermetallics during DC casting and homogenization of an Al-Mg-Si Al Alloy. Metall. Mater. Trans. A 47, 3000–3014.
Lebon, G.S.B., Lazaro-Nebreda, J., Patel, J.B., Fan, Z., 2020. Numerical assessment of in-line rotor–stator mixers in high-shear melt conditioning (HSMC) technology. JOM 72, 4092–4100.
Li, H.T., Wang, Y., Fan, Z., 2012. Mechanisms of enhanced heterogeneous nucleation during solidification in binary Al–Mg alloys. Acta Mater. 60, 1528–1537.
Li, H.T., Zhao, P., Yang, R., Patel, J.B., Chen, X., Fan, Z., 2017. Grain refinement and improvement of solidification defects in direct-chill cast billets of A4032 alloy by melt conditioning. Metall. Mater. Trans. B 48, 2481–2492.
McCartney, D.G., 1989. Grain refining of aluminium and its alloys using inoculants. Int. Mater. Rev. 34, 247–260.
Nadella, R., Eskin, D.G., Du, Q., Katgerman, L., 2008. Macrosegregation in direct-chill casting of aluminium alloys. Prog. Mater. Sci. 53, 421–480.
Nilam, S.B., Ivan, S., Carla, B., Fan, Z., Martin, J., 2021. Enhancement of chip breakability of aluminium alloys by controlling the solidification during direct chill casting. J. Alloys Compd. 862, 158008.
Patel, J.B., Li, H.T., Xia, M.X., Jones, S., Kumar, S., O'Reilly, K., Fan, Z., 2014. Melt conditioned direct chill casting (MC-DC) process for production of high quality aluminium alloy billets. Mater. Sci. Forum. 794–796, 149–154.
Patel, J.B., Yang, X., Mendis, C.L., Fan, Z., 2017. Melt conditioning of light metals by application of high shear for improved microstructure and defect control. JOM 69, 1071–1076.
Pradip, K.S., 2000. Aluminum Extrusion Technology. ASM International, Ohio, pp. 136–137.
Qiu, D., Taylor, J.A., Zhang, M.X., Kelly, P.M., 2007. A mechanism for the poisoning effect of silicon on the crystal refinement of Al-Si alloys. Acta Mater. 55, 1447–1456.
Quested, T.E., Greer, A.L., 2004. The effect of the size distribution of inoculant particles on as-cast grain size in aluminium alloys. Acta Mater. 52, 3859–3868.
Rappaz, M., Boettinger, W.J., 1999. On dendritic solidification of multicomponent alloys with unequal liquid diffusion coefficients. Acta Mater. 47, 3205–3219.
Sengupta, J., Thomas, B.G., Wells, M.A., 2005. The use of water cooling during the continuous casting of steel and aluminum alloys. Metall. Mater. Trans. A 36, 187–204.
Spear, R.E., Gardner, G.R., 1963. Dendrite cell size. Trans. AFS. 71, 209–215.
Vanja, Hatic., Boštjan, Mavric., Nejc, Košnik., Božidar, Šarler., 2018. Simulation of direct chill casting under the influence of a low-frequency electromagnetic field. Appl. Math. Modell. 54, 170–188.
Wang, Y., Fang, C.M., Zhou, L., Hashimoto, T., Zhou, X., Ramasse, Q.M., Fan, Z., 2019. Mechanism for Zr poisoning of Al-Ti-B based grain refiners. Acta Mater. 164, 428–439.
Zuo, Y.B., Cui, J.Z., Zhao, Z.H., Zhang, H.T., Li, L., Zhu, Q.F., 2012. Mechanism of grain refinement of an Al–Zn–Mg–Cu alloy prepared by low-frequency electromagnetic casting. J. Mater. Sci. 47, 5501–5508.